

1 **REVISION 1**

2  
3 **Chromo-alumino-povondraite,  $\text{NaCr}_3(\text{Al}_4\text{Mg}_2)(\text{Si}_6\text{O}_{18})(\text{BO}_3)_3(\text{OH})_3\text{O}$ , a new**  
4 **mineral species of the tourmaline supergroup**

5  
6  
7 LEONID REZNITSKII<sup>1</sup>, CHRISTINE M. CLARK<sup>2</sup>, FRANK C. HAWTHORNE<sup>2,\*</sup>, JOEL D. GRICE<sup>3</sup>,  
8 HENRIK SKOGBY<sup>4</sup>, ULF HÅLENIUS<sup>4</sup> AND FERDINANDO BOSI<sup>4,5,\*</sup>

9  
10  
11 <sup>1</sup>Institute of the Earth's Crust, Siberian Branch, Russian Academy of Science, Lermontova str., 128,  
12 664033 Irkutsk, Russia

13 <sup>2</sup>Department of Geological Sciences, University of Manitoba, Winnipeg, Manitoba R3T 2N2, Canada

14 <sup>3</sup>Research Division, Canadian Museum of Nature, P.O. Box 3443A, Station "D", Ottawa, Ontario,  
15 Canada, K1P 6P4

16 <sup>4</sup>Department of Geosciences, Swedish Museum of Natural History, Box 50007, SE-10405 Stockholm,  
17 Sweden

18 <sup>5</sup>Dipartimento di Scienze della Terra, Sapienza Università di Roma, Piazzale Aldo Moro, 5, I-00185  
19 Rome, Italy

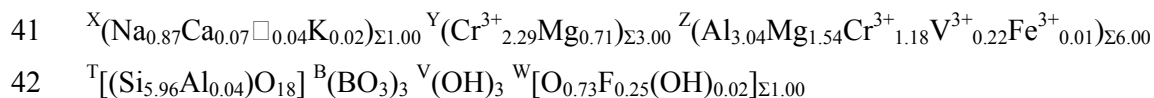
20  
21  
22 \* E-mail: [frank\\_hawthorne@umanitoba.ca](mailto:frank_hawthorne@umanitoba.ca); [ferdinando.bosi@uniroma1.it](mailto:ferdinando.bosi@uniroma1.it)

23  
24  
25  
26  
27 **ABSTRACT**

28 Chromo-alumino-povondraite,  $\text{NaCr}_3(\text{Al}_4\text{Mg}_2)(\text{Si}_6\text{O}_{18})(\text{BO}_3)_3(\text{OH})_3\text{O}$ , is a new mineral  
29 of the tourmaline supergroup. It is found in metaquartzites of the Pereval marble quarry  
30 (Sludyanka, Lake Baikal, Russia) in association with dravite, oxy-chromium-dravite, oxy-  
31 dravite, quartz, calcite, chromphyllite, eskolaite, chromite, uvarovite, chromian phlogopite,

32 and pyroxenes of the diopside-kosmochlor series, Cr-bearing tremolite, Cr-bearing titanite, Cr-  
33 bearing rutile, and pyrite.

34 Crystals are green and transparent with a vitreous luster, and exhibit a pale-green streak  
35 and conchoidal fracture. Chromo-alumino-povondraite has a Mohs hardness of approximately  
36  $7\frac{1}{2}$ , and a calculated density of  $3.227 \text{ g/cm}^3$ . In plane-polarized light, chromo-alumino-  
37 povondraite is pleochroic ( $O$  = emerald green and  $E$  = pale yellowish green) and uniaxial  
38 negative:  $\omega = 1.745(5)$ ,  $\varepsilon = 1.685(5)$ . Chromo-alumino-povondraite is rhombohedral, space  
39 group  $R3m$ , with the unit-cell parameters  $a = 16.0277(2)$ ,  $c = 7.3085(1) \text{ \AA}$ ,  $V = 1625.93(5) \text{ \AA}^3$ ,  
40  $Z = 3$ . Crystal-chemical analysis resulted in the empirical structural formula:



43 The crystal structure of chromo-alumino-povondraite was refined to an  $R1$  index of  
44 1.68% using 1803 unique reflections collected with  $\text{MoK}\alpha$  X-radiation. Ideally, chromo-  
45 alumino-povondraite is related to oxy-dravite and oxy-chromium-dravite by the homovalent  
46 substitution  $\text{Cr}^{3+} \leftrightarrow \text{Al}^{3+}$ . Tourmaline with chemical compositions classified as chromo-  
47 alumino-povondraite can be either Al-dominant or Cr-dominant as a result of the  
48 compositional boundaries along the solid solution between Al and  $\text{Cr}^{3+}$  that are determined at  
49  $^{Y+Z}(\text{Cr}_{1.5}\text{Al}_{5.5})$ , corresponding to  $\text{Na}^Y(\text{Cr}_{1.5}\text{Al}_{1.5})^Z(\text{Al}_4\text{Mg}_2)\text{Si}_6\text{O}_{18}(\text{BO}_3)_3(\text{OH})_3\text{O}$ , and  
50  $^{Y+Z}(\text{Cr}_5\text{Al}_2)$ , corresponding to  $\text{Na}^Y(\text{Cr}_3)^Z(\text{Cr}_2\text{Al}_2\text{Mg}_2)\text{Si}_6\text{O}_{18}(\text{BO}_3)_3(\text{OH})_3\text{O}$ .

51

52

53

## INTRODUCTION

54 The tourmaline supergroup minerals are widespread, occurring in sedimentary, igneous  
55 and metamorphic rocks (Dutrow and Henry 2011). They are important indicator minerals that  
56 can provide information on the compositional evolution of their host rocks, chiefly due to their  
57 ability to incorporate a large number of elements (e.g., Novák et al. 2004; Agrosi et al. 2006;  
58 Lussier et al. 2011a; Novák et al. 2011; van Hinsberg et al. 2011; Bačík et al. 2012). However,  
59 the chemical composition of tourmalines is also controlled by short-range and long-range  
60 constraints (e.g., Hawthorne 1996, 2002; Bosi and Lucchesi 2007; Bosi 2010, 2011; Henry  
61 and Dutrow 2011; Skogby et al. 2012; Bosi 2013). Tourmaline supergroup minerals are  
62 complex borosilicates and their crystal structure and crystal chemistry have been extensively  
63 studied (e.g., Foit 1989; Hawthorne and Henry 1999; Bosi and Lucchesi 2007; Lussier et al.  
64 2008; Bosi 2008; Bosi et al. 2010; Lussier et al. 2011b; Filip et al. 2012). In accordance with

65 Henry et al. (2011), the general formula of tourmaline may be written as:  
66  $XY_3Z_6T_6O_{18}(BO_3)_3V_3W$ , where  $X (\equiv [9]X) = Na^+, K^+, Ca^{2+}, \square$  (=vacancy);  $Y (\equiv [6]Y) = Al^{3+},$   
67  $Fe^{3+}, Cr^{3+}, V^{3+}, Mg^{2+}, Fe^{2+}, Mn^{2+}, Li^+$ ;  $Z (\equiv [6]Z) = Al^{3+}, Fe^{3+}, Cr^{3+}, V^{3+}, Mg^{2+}, Fe^{2+}$ ;  $T (\equiv [4]T)$   
68  $= Si^{4+}, Al^{3+}, B^{3+}$ ;  $B (\equiv [3]B) = B^{3+}$ ;  $W (\equiv [3]O1) = OH^{1-}, F^{1-}, O^{2-}$ ;  $V (\equiv [3]O3) = OH^{1-}, O^{2-}$  and  
69 where, for example,  $T$  represents a group of cations ( $Si^{4+}, Al^{3+}, B^{3+}$ ) accommodated at the [4]-  
70 coordinated  $T$  sites. The dominance of these ions at one or more sites of the structure gives rise  
71 to a range of distinct mineral species.

72 Recently, several new minerals of the tourmaline supergroup were approved by the  
73 Commission on New Minerals, Nomenclature and Classification (CNMNC) of the  
74 International Mineralogical Association (IMA). Among these are a number of oxy-tourmalines  
75 related by complete solid solution in the  $Al^{3+}-Cr^{3+}-V^{3+}$  subsystem: oxy-dravite, end-member  
76 formula  $NaAl_3(Al_4Mg_2)(Si_6O_{18})(BO_3)_3(OH)_3O$  (IMA 2012-004a; Bosi and Skogby 2013),  
77 oxy-chromium-dravite,  $NaCr_3(Cr_4Mg_2)(Si_6O_{18})(BO_3)_3(OH)_3O$  (IMA 2011-097; Bosi et al.  
78 2012a); oxy-vanadium-dravite,  $NaV_3(V_4Mg_2)(Si_6O_{18})(BO_3)_3(OH)_3O$  (IMA 11-E; Bosi et al.  
79 2013a); vanadio-oxy-dravite,  $NaV_3(Al_4Mg_2)(Si_6O_{18})(BO_3)_3(OH)_3O$  (IMA 2012-074; Bosi et  
80 al. 2014a); vanadio-oxy-chromium-dravite,  $NaV_3(Cr_4Mg_2)(Si_6O_{18})(BO_3)_3(OH)_3O$  (IMA 2012-  
81 034; Bosi et al. 2014b).

82 Chromo-alumino-povondraite was originally approved as a new species by the IMA  
83 CNMNC in 2009 (no. 2009-088). Subsequent additional work connected with publication of  
84 the resultant paper showed that the chemical analysis associated with the original proposal was  
85 not reliable. Further work uncovered an appropriate sample with the requisite chemical  
86 composition for this species. Consultation with the Chair of CNMNC resulted in a new  
87 proposal which involved changing the holotype sample. The original approval of IMA 2009-  
88 088 was hence withdrawn on 30 January 2013 (Williams et al. 2013), and a new proposal was  
89 submitted and approved by the IMA-CNMC (no. 2013-089). The holotype specimen (sample  
90 PR85v) is deposited in the collections of the Museum of Mineralogy, Earth Sciences  
91 Department, Sapienza University of Rome, Italy, catalogue number 33069/1. A formal  
92 description of the new species chromo-alumino-povondraite is presented here, including a full  
93 characterization of its physical, chemical and structural properties.

94  
95  
96

#### OCURRENCE, APPEARANCE AND PHYSICAL AND OPTICAL PROPERTIES



129 transform infrared and optical-absorption spectra, refractive indices and X-ray powder  
130 diffraction data were recorded on coexisting crystals. Small differences in composition are  
131 likely to occur between these crystals, as well as minor variations in chemistry within the  
132 crystal population.

133

#### 134 **Single-crystal structural refinement**

135 A representative fragment of the type specimen was selected for X-ray diffraction  
136 measurements on a Bruker KAPPA APEX-II single-crystal diffractometer, at Sapienza  
137 University of Rome (Earth Sciences Department), equipped with a CCD area detector ( $6.2 \times$   
138  $6.2 \text{ cm}^2$  active detection area,  $512 \times 512$  pixels) and a graphite crystal monochromator, using  
139 MoK $\alpha$  radiation from a fine-focus sealed X-ray tube. The sample-to-detector distance was 4  
140 cm. A total of ca. 3265 exposures (step =  $0.2^\circ$ , time/step = 20 s) covering a full reciprocal  
141 sphere with a redundancy of about 8 was used. Final unit-cell parameters were refined using  
142 the Bruker AXS SAINT program for reflections with  $I > 10 \sigma(I)$  in the range  $5^\circ < 2\theta < 72^\circ$ .  
143 The intensity data were processed and corrected for Lorentz, polarization, and background  
144 effects with the APEX2 software program of Bruker AXS. The data were corrected for  
145 absorption using the multi-scan method (SADABS). The absorption correction led to a  
146 significant improvement in  $R_{\text{int}}$ . No violations of  $R3m$  symmetry were noted.

147 Structural refinement was done with the SHELXL-97 program (Sheldrick 2008).  
148 Starting coordinates were taken from Bosi et al. (2004). Variable parameters were: scale  
149 factor, extinction coefficient, atom coordinates, site-scattering values and atom-displacement  
150 factors. To obtain the best values of statistical indexes ( $R1$ ,  $wR2$ ), a fully ionized scattering  
151 curve for O was used, whereas neutral scattering curves were used for the other atoms. In  
152 detail, the occupancy of the  $X$  site was modeled by using the Na scattering factor, and both the  
153  $Y$  and  $Z$  sites using Cr and Mg scattering factors. The  $T$  and  $B$  sites were modeled,  
154 respectively, with Si and B scattering factors and with a fixed occupancy of 1, because  
155 refinement with unconstrained occupancies showed no significant deviations from this value.  
156 Three full-matrix refinement cycles with isotropic-displacement parameters for all atoms were  
157 followed by anisotropic cycles until convergence was attained. No significant correlations  
158 over a value of 0.7 between the parameters were observed at the end of refinement. Table 1  
159 lists crystal data, data-collection information and refinement details; Table 2 gives the  
160 fractional atom coordinates and site occupancies; Table 3 gives the displacement parameters;  
161 Table 4 gives selected bond distances.

162

### 163 **X-ray powder diffraction**

164 X-ray powder data were collected with a Bruker D8 Discover SuperSpeed micro-  
165 powder diffractometer with multi-wire 2D detector using a modified Gandolfi attachment  
166 (CuK $\alpha$  radiation,  $\lambda = 1.54178 \text{ \AA}$ , 50 kV, 60 mA). Two 10 h frames were collected and merged;  
167 no internal standard was used. Data listed in Table 5 are indexed on  $a = 16.095(17)$ ,  $c =$   
168  $7.341(9) \text{ \AA}$ .

169

### 170 **Electron-Microprobe analysis**

171 Electron-microprobe analyses of the crystal used for X-ray diffraction refinement were  
172 obtained by wavelength-dispersive spectrometry (WDS mode) with a Cameca SX50  
173 instrument at the “Istituto di Geologia Ambientale e Geoingegneria (Rome, Italy), CNR”,  
174 operating at an accelerating potential of 15 kV and a sample current of 15 nA, 10  $\mu\text{m}$  beam  
175 diameter. Minerals and synthetic compounds were used as standards: wollastonite (Si, Ca),  
176 magnetite (Fe), rutile (Ti), corundum (Al), vanadinite (V) fluorphlogopite (F), periclase (Mg),  
177 jadeite (Na), K-feldspar (K), sphalerite (Zn), metallic Cr, Mn and Cu. The overlap corrections  
178 and the PAP routine were applied (Pouchou and Pichoir 1991). The results (Table 6) represent  
179 mean values of 10 spot analyses. In accord with the very low concentration of Li in dravitic  
180 samples (e.g., Henry et al. 2011) and the crystallization environment of the studied sample  
181 (i.e., Cr-bearing metaquartzites), the Li<sub>2</sub>O content was assumed to be insignificant.  
182 Manganese, Zn, Cu and Ti were below the detection limits (0.03 wt%) in the studied sample.

183

### 184 **Infrared spectroscopy**

185 A homogeneous chromo-alumino-povondraite crystal from the holotype material was  
186 measured by Fourier-transform infrared (FTIR) absorption spectroscopy in the wavenumber  
187 range 2000-5000  $\text{cm}^{-1}$  to characterize OH absorption bands, using a Bruker Equinox 55  
188 spectrometer equipped with a tungsten-halogen source and a CaF<sub>2</sub> beam-splitter. Polarized  
189 spectra with a resolution of 4  $\text{cm}^{-1}$  were acquired parallel and perpendicular to the  
190 crystallographic **c**-axis direction using an IR microscope with a KRS-5 wire-grid polarizer and  
191 an MCT detector. The 26  $\mu\text{m}$  thick doubly-polished crystal plate had been oriented parallel the  
192 **c**-axis by morphology and optical microscopy. As normally observed, it was not possible to

193 thin the sample sufficiently to avoid off-scale absorption intensity for the strongest band (Fig.  
194 1).

195

### 196 **Optical-absorption spectroscopy**

197 Polarized, room-temperature optical-absorption spectra (OAS) were recorded on the  
198 same 26  $\mu\text{m}$  thick crystal platelet used for the FTIR measurements. The spectra were  
199 measured in the range 300-1100 nm at a resolution of 1 nm using an AVASPEC-  
200 ULS2048X16 spectrometer attached via a 400  $\mu\text{m}$  UV optical fiber to a Zeiss Axiotron UV-  
201 microscope. A 75 W Xenon arc lamp served as illuminating source and Zeiss Ultrafluar 10x  
202 lenses served as objective and condenser. A UV-quality Glan-Thompson prism with a working  
203 range from 250 to 2700 nm ( $40000$  to  $3704\text{ cm}^{-1}$ ) was used as a polarizer. The circular  
204 aperture was 64  $\mu\text{m}$  in diameter. The wavelength scale of the spectrometer was calibrated  
205 against  $\text{Ho}_2\text{O}_3$  doped and  $\text{Pr}_2\text{O}_3/\text{Nd}_2\text{O}_3$  doped standards (Hellma glass filters 666F1 and  
206 666F7) with an accuracy better than  $15\text{ cm}^{-1}$  in the wavelength range 300-1100 nm. Recorded  
207 spectra were fitted using the Jandel PeakFit 4.12 software assuming Gaussian peak shapes.

208

209

## RESULTS AND DISCUSSION

### 210 **Determination of atomic proportions**

211 In agreement with the structural-refinement results, the boron content was assumed to  
212 be stoichiometric in the chromo-alumino-povondraite sample ( $\text{B}^{3+} = 3.00$  apfu). Both the site-  
213 scattering results and the bond lengths of *B* and *T* are consistent with the *B* site fully occupied  
214 by boron and no amount of  $\text{B}^{3+}$  at the *T* site (e.g., Hawthorne 1996; Bosi and Lucchesi 2007).  
215 The small contents of Fe were calculated as  $\text{Fe}^{3+}$ , on the basis of results of (Bosi et al. 2013b).  
216 The (OH) content can then be calculated by charge balance with the assumption  $T + Y + Z =$   
217 15.00. The atomic proportions were calculated on this assumption (Table 6). The excellent  
218 match between the number of electrons per formula unit (epfu) derived from chemical and  
219 structural analysis supports this procedure, respectively: 265.6 and 266.3 epfu.

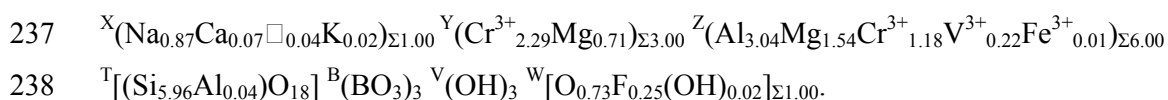
220

### 221 **Site populations**

222 The anion site populations in the studied sample follow the general preference  
223 suggested for tourmaline (e.g., Grice and Ercit 1993; Henry et al. 2011): the O3 site (V  
224 position in the general formula) is occupied by (OH), and the O1 site (W position in the  
225 general formula) is occupied by  $\text{O}^{2-}$ ,  $(\text{OH})^{1-}$  and  $\text{F}^{1-}$ . The cation distribution at the *T*, *Y* and *Z*

226 sites was optimized by using a quadratic program to minimize the residuals between calculated  
227 and observed data (based on the chemical and structural analysis). Site-scattering values,  
228 octahedral and tetrahedral mean bond-distances (i.e.,  $\langle Y-O \rangle$ ,  $\langle Z-O \rangle$  and  $\langle T-O \rangle$ ) were  
229 calculated as the linear contribution of each cation multiplied by its ideal bond-distance (Table  
230 7). More details about the ideal distances as well as the optimization procedure may be found  
231 in Bosi et al. (2004) and Bosi and Lucchesi (2004; 2007). The robustness of this approach was  
232 confirmed by another optimization procedure (Wright et al. 2000), which led to very similar  
233 cation distributions (Table 7). This result represents another example of convergence of these  
234 two procedures to similar solutions for tourmaline (e.g., Bosi and Lucchesi 2007; Filip et al.  
235 2012; Bosi et al. 2012a, 2013a; Bosi and Skogby 2013).

236 The final structural formula is as follows:



239 The bond-valence analysis is consistent with the optimized structural formulae. Bond-valence  
240 sums (BVS), using the formula and bond-valence parameters from Brown and Altermatt  
241 (1985), are reported in Table 8. In this regard, note that the equation for the  $^W(\text{OH})$  calculation  
242 [reported by Bosi (2013),  $^W(\text{OH}) = 2 - 1.01 \text{ BVS}(\text{O1}) - 0.21 - \text{F}$ ] yields an  $^W(\text{OH})$  value very  
243 close to that of the empirical formula: 0.03 apfu and 0.02 apfu, respectively.

244

### 245 **Name and crystal chemistry**

246 The composition of the present sample PR85v is consistent with a tourmaline  
247 belonging to the alkali group, oxy-subgroup 3 (Henry et al. 2011): Na-dominant at the X  
248 position of the general formula of tourmaline  $\text{XY}_3\text{Z}_6\text{T}_6\text{O}_{18}(\text{BO}_3)_3\text{V}_3\text{W}$  and oxygen-dominant  
249 at W with  $\text{O}^{2-} > (\text{OH}+\text{F})$ . As  $\text{Cr}^{3+}$  is the dominant cation at Y and  $\text{Al}^{3+}$  is the dominant cation  
250 at Z, its end-member composition may be represented as  $\text{NaCr}_3(\text{Al}_4\text{Mg}_2)\text{Si}_6\text{O}_{18}(\text{BO}_3)_3(\text{OH})_3\text{O}$ .  
251 Although tourmaline chemical compositions compatible with that of the studied sample were  
252 already reported in the literature (samples TMT6b, TMT3c, TMpr79f and TM1p43e of Bosi et  
253 al. 2004), no samples have yet been formally defined as  $\text{Cr}^{3+}$ - and  $\text{Al}^{3+}$ -dominant at Y and Z  
254 (respectively). Therefore, the present tourmaline can be classified as a new species. Its closest  
255 end-member composition of a valid tourmaline species is that of oxy-dravite. The name  
256 chromo-alumino-povondraite is the same as the original name given in the 2009-088 proposal.

257 Although there exists a significant degree of  $\text{Cr}^{3+}$  and Mg disorder over the Y and Z  
258 sites, the structural formula of sample PR85v indicates a preference of  $\text{Cr}^{3+}$  for the Y site and



259 Mg for the Z site. Aluminum, on the other hand, is completely ordered at the Z site. The O1  
260 site is dominated by  $O^{2-}$  with a significant concentration of F (0.25 apfu) and a minor  
261 concentration of (OH). The presence of only minor concentrations of (OH) at O1 (~0.02 apfu)  
262 are consistent with the observation of weak absorption bands at 3720 and 3760  $cm^{-1}$  in the  
263 infrared spectrum (Fig. 1), i.e. the area typically ascribed to the O1 site (see below).

264

### 265 **Infrared spectroscopy**

266 Spectra recorded in polarized mode perpendicular and parallel to the crystallographic **c**  
267 axis show an intense broad band around 3530  $cm^{-1}$  and two weak bands at 3720 and 3760  $cm^{-1}$ ,  
268 all strongly polarized in the **c** direction (Fig. 1). As it was not possible to thin the sample  
269 sufficiently to avoid off-scale absorption for the main band in the **c**-axis direction, any possible  
270 fine structure cannot be discerned. However, in line with previous studies (Bosi et al. 2012b;  
271 Bosi et al. 2013b), the band can be related to the local arrangement  $({}^YCr^{3+} {}^ZR {}^ZR)-O3$ , i.e., to  
272 the occurrence of (OH) at the V position of the tourmaline general formula (O3 site in the  
273 structure). The two weak bands at ca. 3720 and 3760  $cm^{-1}$  are consistent with the minor  
274 concentrations of (OH) (ca. 0.02 apfu) assigned to the W position (O1 site in the structure),  
275 and may be related to the local arrangements  ${}^Y(Mg Mg Mg)$  and  ${}^Y(Mg Mg R^{3+})$  (cf. Gonzalez-  
276 Carreño et al. 1988; Bosi et al. 2012b; Bosi et al. 2013b).

277

### 278 **Optical-absorption spectroscopy**

279 The optical spectra of chromo-alumino-povondraite show two broad absorption bands  
280 at ca. 435 and 590 nm, superimposed on an intense UV absorption edge (Fig. 3). These  
281 absorption bands are ascribed to spin-allowed *d-d* transitions in octahedrally coordinated  $Cr^{3+}$ ,  
282 in accord with comparable bands at ca. 430 and 590 nm observed in spectra of Fe-bearing  
283 chromo-alumino-povondraite (Bosi et al. 2013b) as well as bands observed in spectra of other  
284 Cr-bearing tourmalines (Manning 1969; Taran et al. 1993; Ertl et al. 2008).

285

286

287

### **RELATION TO THE OTHER SPECIES**

288 Chromo-alumino-povondraite  $[NaCr_3(Al_4Mg_2)Si_6O_{18}(BO_3)_3(OH)_3O]$  is related to oxy-  
289 dravite  $[NaAl_3(Al_4Mg_2)Si_6O_{18}(BO_3)_3(OH)_3O]$ , in the ordered form] by the substitution  $3Cr^{3+} \rightarrow$   
290  $3Al$ , and to oxy-chromium-dravite  $[NaCr_3(Cr_4Mg_2)Si_6O_{18}(BO_3)_3(OH)_3O]$  by the substitution  
291  $4Al \rightarrow 4Cr^{3+}$ . The properties of these three tourmalines are compared in Table 9.

292 Figure 3 displays the ternary diagram of the  $V_{\text{total}}\text{-Cr}_{\text{total}}\text{-Al}_{\text{total}}$  system for oxy(O1)-  
293 tourmaline  $\text{Na}^Y(\text{R}^{3+})_3\text{Z}(\text{R}^{3+}_4\text{Mg}_2)\text{Si}_6\text{O}_{18}(\text{BO}_3)_3(\text{OH})_3\text{O}$  (where  $\text{R}^{3+} = \text{V}, \text{Cr}, \text{Al}$ ) showing the  
294 position of the studied sample and that of ideal chromo-alumino-povondraite. This species  
295 occurs between the series oxy-chromium-dravite and oxy-dravite, its compositional limits  
296 were calculated by Bosi et al. (2013b) at  $Y+Z(\text{Cr}_{1.5}\text{Al}_{5.5})$ , corresponding to  
297  $\text{Na}^Y(\text{Cr}_{1.5}\text{Al}_{1.5})\text{Z}(\text{Al}_4\text{Mg}_2)\text{Si}_6\text{O}_{18}(\text{BO}_3)_3(\text{OH})_3\text{O}$  towards to oxy-dravite, and  $Y+Z(\text{Cr}_5\text{Al}_2)$ ,  
298 corresponding to  $\text{Na}^Y(\text{Cr}_3)\text{Z}(\text{Cr}_2\text{Al}_2\text{Mg}_2)\text{Si}_6\text{O}_{18}(\text{BO}_3)_3(\text{OH})_3\text{O}$  toward to oxy-chromium-  
299 dravite. In a similar way, the compositional limits of vanadio-oxy-chromium-dravite and  
300 vanadio-oxy-dravite were inferred (Bosi et al. 2014a,b).

301

302

### IMPLICATIONS

303 The discovery of the new mineral chromo-alumino-povondraite provides new  
304 information on the crystal chemistry of the tourmaline supergroup. The current chemical data  
305 supports complete solid-solution of  $\text{V}^{3+}$ ,  $\text{Cr}^{3+}$  and Al in species of the tourmaline supergroup  
306 (Reznitsky et al. 2001; Bosi et al. 2004, 2013a,b, Bosi 2014a,b) showing that tourmaline with  
307 chemical compositions classified as chromo-alumino-povondraite can be either Al-dominant  
308 or Cr-dominant as a result of the compositional boundaries along the solid solution between Al  
309 and Cr.

310

311

### ACKNOWLEDGMENTS

312 Chemical analyses were done with the kind assistance of Marcello Serracino to whom  
313 the authors express their gratitude. Leonid Reznitskii was supported by a grant from the  
314 Russian Foundation for Basic Research (project 13-05-00258). Frank Hawthorne was  
315 supported by a Canada Research Chair in Crystallography and Mineralogy and by Discovery,  
316 Equipment and Major Installation grants of the Natural Sciences and Engineering Research  
317 Council of Canada, and by Innovation grants from the Canada Foundation for Innovation. The  
318 review of Darrell Henry and an anonymous referee as well as the handling of the AE Aaron  
319 Celestian is acknowledged.

320

321

322

### REFERENCES CITED

- 323 Agrosi, G., Bosi, F., Lucchesi, S., Melchiorre, G., and Scandale, E. (2006) Mn-tourmaline  
324 crystals from island of Elba (Italy): Growth history and growth marks. American  
325 Mineralogist, 91, 944-952.
- 326 Bačík P., Méres Š., and Uher P. (2011) Vanadium-bearing tourmaline in metacherts from  
327 Chvojnice, Slovak Republic: crystal chemistry and multistage evolution. Canadian  
328 Mineralogist, 49, 195-206.
- 329 Bačík, P., Uher, P., Ertl, A., Jonsson, E., Nysten, P., Kanický, V., and Vaculovič, T. (2012)  
330 Zoned REE Enriched Dravite from a Granitic Pegmatite in Forshammar Bergslagen  
331 Province, Sweden an EMPA, XRD and LA-ICP-MS study. Canadian Mineralogist. 50,  
332 825-841.
- 333 Bosi, F. (2008) Disordering of Fe<sup>2+</sup> over octahedrally coordinated sites of tourmaline.  
334 American Mineralogist, 93, 1647-1653.
- 335 Bosi, F. (2010) Octahedrally coordinated vacancies in tourmaline: a theoretical approach.  
336 Mineralogical Magazine, 74, 1037-1044.
- 337 Bosi, F. (2011) Stereochemical constraints in tourmaline: from a short-range to a long-range  
338 structure. Canadian Mineralogist, 49, 17-27.
- 339 Bosi, F. (2013) Bond-valence constraints around the O1 site of tourmaline. Mineralogical  
340 Magazine, 77, 343-351.
- 341 Bosi, F., and Lucchesi, S. (2004) Crystal chemistry of the schorl-dravite series. European  
342 Journal of Mineralogy, 16, 335-344.
- 343 Bosi, F., and Lucchesi, S. (2007) Crystal chemical relationships in the tourmaline group:  
344 structural constraints on chemical variability. American Mineralogist, 92, 1054-1063.
- 345 Bosi, F., and Skogby, H. (2013) Oxy-dravite, Na(Al<sub>2</sub>Mg)(Al<sub>5</sub>Mg)(Si<sub>6</sub>O<sub>18</sub>)(BO<sub>3</sub>)<sub>3</sub>(OH)<sub>3</sub>O, a  
346 new mineral species of the tourmaline supergroup. American Mineralogist, 98, 1442-  
347 1448.
- 348 Bosi F., Lucchesi, S., and Reznitskii, L. (2004) Crystal chemistry of the dravite-chromdravite  
349 series. European Journal of Mineralogy, 16, 345-352.
- 350 Bosi, F., Balić-Žunić, T., and Surour, A.A. (2010) Crystal structure analysis of four  
351 tourmalines from the Cleopatra's Mines (Egypt) and Jabal Zalm (Saudi Arabia), and the  
352 role of Al in the tourmaline group. American Mineralogist, 95, 510-518.
- 353 Bosi, F., Reznitskii, L., and Skogby, H. (2012a) Oxy-chromium-dravite,  
354 NaCr<sub>3</sub>(Cr<sub>4</sub>Mg<sub>2</sub>)(Si<sub>6</sub>O<sub>18</sub>)(BO<sub>3</sub>)<sub>3</sub>(OH)<sub>3</sub>O, a new mineral species of the tourmaline  
355 supergroup. American Mineralogist, 97, 2024-2030.

- 356 Bosi, F., Skogby, H., Agrosi, G., and Scandale, E. (2012b) Tsilaisite,  
357  $\text{NaMn}_3\text{Al}_6(\text{Si}_6\text{O}_{18})(\text{BO}_3)_3(\text{OH})_3\text{OH}$ , a new mineral species of the tourmaline supergroup  
358 from Grotta d'Oggi, San Pietro in Campo, island of Elba, Italy. *American Mineralogist*,  
359 97, 989-994.
- 360 Bosi, F., Reznitskii, L., and Sklyarov, E.V. (2013a) Oxy-vanadium-dravite,  
361  $\text{NaV}_3(\text{V}_4\text{Mg}_2)(\text{Si}_6\text{O}_{18})(\text{BO}_3)_3(\text{OH})_3\text{O}$ : crystal structure and redefinition of the  
362 "vanadium-dravite" tourmaline. *American Mineralogist*. 98, 501-505.
- 363 Bosi, F., Skogby, H., Hålenius, U., and Reznitskii, L. (2013b) Crystallographic and  
364 spectroscopic characterization of Fe-bearing chromo-alumino-povondraite and its  
365 relations with oxy-chromium-dravite and oxy-dravite. *American Mineralogist*, 98, 1557-  
366 1564.
- 367 Bosi, F., Skogby, H., Reznitskii, L., and Hålenius, U. (2014a) Vanadio-oxy-dravite,  
368  $\text{NaV}_3(\text{Al}_4\text{Mg}_2)(\text{Si}_6\text{O}_{18})(\text{BO}_3)_3(\text{OH})_3\text{O}$ , a new mineral species of the tourmaline  
369 supergroup. *American Mineralogist*, 99, 218-224.
- 370 Bosi, F., Reznitskii, L., Skogby, H., and Hålenius, U. (2014b) Vanadio-oxy-chromium-dravite,  
371  $\text{NaV}_3(\text{Cr}_4\text{Mg}_2)(\text{Si}_6\text{O}_{18})(\text{BO}_3)_3(\text{OH})_3\text{O}$ , a new mineral species of the tourmaline  
372 supergroup. *American Mineralogist*, 99, [dx.doi.org/10.2138/am.2014.4568](http://dx.doi.org/10.2138/am.2014.4568).
- 373 Brown, I.D., and Altermatt, D. (1985) Bond-valence parameters obtained from a systematic  
374 analysis of the Inorganic Crystal Structure Database. *Acta Crystallographica*, B41, 244-  
375 247.
- 376 Dutrow, B.L., and Henry, D.J. (2011) Tourmaline: A geologic DVD. *Elements*, 7(5), 301-306.
- 377 Ertl, A., Rossman, G.R., Hughes, J.M., Ma, C., and Brandstätter, F. (2008)  $\text{V}^{3+}$ -bearing, Mg-  
378 rich strongly disordered olenite from a graphite deposit near Amstall, Lower Austria: A  
379 structural, chemical and spectroscopic investigation. *Neues Jahrbuch für Mineralogie*  
380 *Abhandlungen*, 184, 243-253.
- 381 Filip, J., Bosi, F., Novák, M., Skogby, H., Tuček, J., Čuda, J., and Wildner, M. (2012) Redox  
382 processes of iron in the tourmaline structure: example of the high-temperature treatment  
383 of  $\text{Fe}^{3+}$ -rich schorl. *Geochimica et Cosmochimica Acta*, 86, 239-256.
- 384 Foit, F.F. Jr. (1989) Crystal chemistry of alkali-deficient schorl and tourmaline structural  
385 relationships. *American Mineralogist*, 74, 422-431.
- 386 Gonzalez-Carreño, T., Fernandez, M., and Sanz, J. (1988) Infrared and electron microprobe  
387 analysis in tourmalines. *Physics and Chemistry of Minerals*, 15, 452-460.

- 388 Grice, J.D., and Ercit, T.S. (1993) Ordering of Fe and Mg in the tourmaline crystal structure:  
389 the correct formula. *Neues Jahrbuch für Mineralogie, Abhandlungen*, 165, 245-266.
- 390 Hawthorne, F.C. (1996) Structural mechanisms for light-element variations in tourmaline.  
391 *Canadian Mineralogist*, 34, 123-132.
- 392 Hawthorne, F. C. (2002) Bond-valence constraints on the chemical composition of tourmaline.  
393 *Canadian Mineralogist*, 40, 789-797.
- 394 Hawthorne, F.C. and Henry, D. (1999) Classification of the minerals of the tourmaline group.  
395 *European Journal of Mineralogy*, 11, 201-215.
- 396 Henry, D.J., and Dutrow, B.L. (2011) The incorporation of fluorine in tourmaline: Internal  
397 crystallographic controls or external environmental influences? *Canadian Mineralogist*,  
398 49, 41-56.
- 399 Henry, D.J., Novák, M., Hawthorne, F.C., Ertl, A., Dutrow, B., Uher, P., and Pezzotta, F.  
400 (2011) Nomenclature of the tourmaline supergroup minerals. *American Mineralogist*, 96,  
401 895-913.
- 402 Kotov, A.B., Salnikova, E.B., Reznitskii, L.Z., Vasil'ev, E.P., Kozakov, I.K., Yakovleva, S.Z.,  
403 Kovach, V.P., and Berezhnaya, N.G. (1997) Age of metamorphism of the Slyudyanka  
404 crystalline complex, Southern Baikal Area: U–Pb geochronology of granitoids.  
405 *Petrology*, 5, 338-349.
- 406 Kovach, V., Salnikova, E., Wang, K-L., Jahn, B-M., Chiu, H-Y., Reznitskiy, L., Kotov, A.,  
407 Iizuka, Y., Chung, S-L. (2013) Zircon ages and Hf isotopic constraints on sources of  
408 clastic metasediments of the Slyudyansky high-grade complex, southeastern Siberia:  
409 Implication for continental growth and evolution of the Central Asian Orogenic Belt.  
410 *Journal of Asian Earth Sciences*, 62. 18-36.
- 411 Lussier, A.J., Aguiar, P.M., Michaelis, V.K., Kroeker, S., Herwig, S., Abdu, Y., and  
412 Hawthorne, F.C. (2008) Mushroom elbaite from the Kat Chay mine, Momeik, near  
413 Mogok, Myanmar: I. Crystal chemistry by SREF, EMPA, MAS NMR and Mössbauer  
414 spectroscopy. *Mineralogical Magazine*, 72, 747-761.
- 415 Lussier, A.J., Hawthorne, F.C., Aguiar, P.M., Michaelis, V.K., and Kroeker, S. (2011a)  
416 Elbaite-liddicoatite from Black Rapids glacier, Alaska. *Periodico di Mineralogia*, 80, 57-  
417 73.
- 418 Lussier, A.J., Abdu, Y. Hawthorne, F.C., Michaelis, V.K., Aguiar, P.M., and Kroeker, S.  
419 (2011b) Oscillatory zoned liddicoatite from Anjanabonoina, central Madagascar. I.

- 420 Crystal chemistry and structure by SREF and  $^{11}\text{B}$  and  $^{27}\text{Al}$  MAS NMR spectroscopy.  
421 Canadian Mineralogist, 49, 63-88.
- 422 Mandarino, J.A. (1976) The Gladstone-Dale relationship. Part I: derivation of new constants.  
423 Canadian Mineralogist, 14, 498-502.
- 424 Mandarino, J.A. (1981) The Gladstone-Dale relationship. Part IV: the compatibility concept  
425 and its application. Canadian Mineralogist, 19, 441-450.
- 426 Manning, P.G. (1969) Optical absorption spectra of chromium-bearing tourmaline, black  
427 tourmaline and buergerite. Canadian Mineralogist, 9, 57-70.
- 428 Novák, M., Povondra, P., and Selway, J.B. (2004) Schorl-oxy-schorl to dravite-oxy-dravite  
429 tourmaline from granitic pegmatites; examples from the Moldanubicum, Czech  
430 Republic. European Journal of Mineralogy, 16, 323-333.
- 431 Novák M., Škoda P., Filip J., Macek I., and Vaculovič T. (2011) Compositional trends in  
432 tourmaline from intragranitic NYF pegmatites of the Třebíč Pluton, Czech Republic;  
433 electron microprobe, Mössbauer and LA-ICP-MS study. Canadian Mineralogist, 49,  
434 359-380.
- 435 Pouchou, J.L., and Pichoir, F. (1991) Quantitative analysis of homogeneous or stratified  
436 microvolumes applying the model "PAP." In K.F.J. Heinrich and D.E. Newbury, Eds.,  
437 Electron Probe Quantitation, p. 31–75. Plenum, New York.
- 438 Reznitsky, L.Z., Sklyarov, E.V., Ushchapovskaya, Z.V., Nartova, N.V., Kashaev, A.A.,  
439 Karmanov, N.S., Kanakin, S.V., Smolin, A.S., and Nekrosova, E.A. (2001)  
440 Vanadiumdravite,  $\text{NaMg}_3\text{V}_6[\text{Si}_6\text{O}_{18}][\text{BO}_3]_3(\text{OH})_4$ , a new mineral of the tourmaline  
441 group. Zapiski Vsesoyuznogo Mineralogicheskogo Obshchestva, 130, 59-72 (in  
442 Russian).
- 443 Salnikova, E.B., Sergeev, S.A., Kotov, A.B., Yakovleva, S.Z., Steiger, R.H., Reznitskiy, L.Z.,  
444 and Vasil'ev, E.P. (1998) U-Pb zircon dating of granulite metamorphism in the  
445 Slyudyanskiy complex, Eastern Siberia. Gondwana Research, 1, 195–205.
- 446 Sheldrick, G.M. (2008) A short history of SHELX. Acta Crystallographica, A64, 112-122.
- 447 Skogby, H., Bosi, F., and Lazor, P. (2012) Short-range order in tourmaline: a vibrational  
448 spectroscopic approach to elbaite. Physics and Chemistry of Minerals, 39, 811-816.
- 449 Taran, M.N., Lebedev, A.S., and Platonov, A.N. (1993) Optical absorption spectroscopy of  
450 synthetic tourmalines. Physics and Chemistry of Minerals, 20, 209-220.
- 451 van Hinsberg, V.J., Henry, D.J., and Marschall, H.R. (2011) Tourmaline: an ideal indicator of  
452 its host environment. Canadian Mineralogist, 49, 1-16.

- 453 Williams, P.A., Hatert, F., Pasero, M., and Mills, S. (2013) New minerals, nomenclature  
454 modifications approved in 2013. *Mineralogical Magazine*, 77, 2695–2709.
- 455 Wright, S.E., Foley, J.A., and Hughes, J.M. (2000) Optimization of site occupancies in  
456 minerals using quadratic programming. *American Mineralogist*, 85, 524-531.

457

458

#### LIST OF TABLES

459 **TABLE 1.** Single-crystal X-ray diffraction data details for chromo-alumino-povondraite.

460 **TABLE 2.** Fractional atom coordinates and site occupancy for chromo-alumino-povondraite.

461 **TABLE 3.** Displacement parameters ( $\text{\AA}^2$ ) for chromo-alumino-povondraite.

462 **TABLE 4.** Selected bond distances ( $\text{\AA}$ ) for chromo-alumino-povondraite.

463 **TABLE 5.** X-ray powder diffraction data for chromo-alumino-povondraite.

464 **TABLE 6.** Chemical composition of chromo-alumino-povondraite.

465 **TABLE 7.** Cation site populations (apfu), mean atomic number and mean bond distances ( $\text{\AA}$ )  
466 for chromo-alumino-povondraite.

467 **TABLE 8.** Bond valence calculations (valence units) for chromo-alumino-povondraite.

468 **TABLE 9.** Comparative data for oxy-dravite, chromo-alumino-povondraite and oxy-chromium-  
469 dravite.

470

471

472

#### LIST OF FIGURES AND FIGURE CAPTIONS

473 **FIGURE 1.** Polarized FTIR absorption spectra in the (OH)-stretching region of chromo-  
474 alumino-povondraite, vertically offset for clarity. Sample thickness 26  $\mu\text{m}$ . The  
475 main band around 3530  $\text{cm}^{-1}$  is truncated in the *c* direction due to excessive  
476 absorption. Spectral ranges expected for bands related to (OH) at the O1 and O3  
477 anion sites are indicated.

478 **FIGURE 2.** Polarized electronic absorption spectra for chromo-alumino-povondraite. Sample  
479 thickness 26  $\mu\text{m}$ .

480 **FIGURE 3.** Ternary diagram of the  $V_{\text{total}}\text{-}Cr_{\text{total}}\text{-}Al_{\text{total}}$  subsystem for oxy-tourmaline  
481  $\text{Na}^Y(R^{3+})_3^Z(R^{3+}_4\text{Mg}_2)\text{Si}_6\text{O}_{18}(\text{BO}_3)_3(\text{OH})_3\text{O}$ . The full black circle is the studied  
482 sample.

483

484



Table 1. Single-crystal X-ray diffraction data details for chromo-alumino-povondraite

Sample	PR85v
Crystal sizes (mm)	0.10 × 0.10 × 0.20
<i>a</i> (Å)	16.0277(2)
<i>c</i> (Å)	7.3085(1)
<i>V</i> (Å <sup>3</sup> )	1625.93(5)
Range for data collection, 2θ (°)	5-72
Reciprocal space range <i>hkl</i>	−26 ≤ <i>h</i> ≤ 15 −26 ≤ <i>k</i> ≤ 26 −11 ≤ <i>l</i> ≤ 10
Total number of frames	3265
Set of measured reflections	7819
Unique reflections, <i>R</i> <sub>int</sub> (%)	1803, 2.02
Redundancy	8
Absorption correction method	SADABS
Refinement method	Full-matrix least-squares on <i>F</i> <sup>2</sup>
Structural refinement program	SHELXL-97
Extinction coefficient	0.00057(8)
Flack parameter	0.05(2)
<i>wR</i> 2 (%)	3.43
<i>R</i> 1 (%) all data	1.68
<i>R</i> 1 (%) for <i>I</i> > 2σ( <i>I</i> )	1.58
GooF	1.055
Largest diff. peak and hole (±e <sup>−</sup> /Å <sup>3</sup> )	−0.39 and 0.34

Notes: *R*<sub>int</sub> = merging residual value; *R*1 = discrepancy index, calculated from *F*-data; *wR*2 = weighted discrepancy index, calculated from *F*<sup>2</sup>-data; GooF = goodness of fit; Diff. Peaks = maximum and minimum residual electron density. Radiation, MoKα = 0.71073 Å. Data collection temperature = 293 K. Space group *R*3*m*; *Z* = 3.

**TABLE 2.** Fractional atom coordinates and site occupancy for chromo-alumino-povondraite

Site	x	y	z	Site occupancy
X	0	0	0.22801(18)	Na <sub>1.044(6)</sub>
Y	0.12380(2)	0.061898(10)	0.63723(5)	Cr <sub>0.767(4)</sub> Mg <sub>0.233(4)</sub>
Z	0.297903(19)	0.261913(19)	0.60938(6)	Cr <sub>0.280(2)</sub> Mg <sub>0.720(2)</sub>
B	0.10993(6)	0.21986(12)	0.4549(2)	B <sub>1.00</sub>
T	0.190426(19)	0.18870(2)	0	Si <sub>1.00</sub>
O1 (≡W)	0	0	0.7661(3)	O <sub>1.00</sub>
O2	0.06037(4)	0.12074(8)	0.48900(15)	O <sub>1.00</sub>
O3 (≡V)	0.25735(9)	0.12868(4)	0.51027(17)	O <sub>1.00</sub>
O4	0.09256(4)	0.18511(9)	0.07144(16)	O <sub>1.00</sub>
O5	0.18285(9)	0.09142(4)	0.09074(15)	O <sub>1.00</sub>
O6	0.19226(6)	0.18294(6)	0.78002(12)	O <sub>1.00</sub>
O7	0.28334(5)	0.28296(5)	0.07444(12)	O <sub>1.00</sub>
O8	0.20763(6)	0.26830(6)	0.43859(13)	O <sub>1.00</sub>
H3	0.2575(16)	0.1287(8)	0.395(3)	H <sub>1.00</sub>

**TABLE 3.** Displacement parameters ( $\text{\AA}^2$ ) for chromo-alumino-povondraite

Site	$U^{11}$	$U^{22}$	$U^{33}$	$U^{23}$	$U^{13}$	$U^{12}$	$U_{\text{eq}}/U_{\text{iso}}^*$
X	0.0212(5)	0.0212(5)	0.0186(7)	0	0	0.0106(2)	0.0203(4)
Y	0.00518(13)	0.00495(10)	0.00650(12)	-0.00037(4)	-0.00074(8)	0.00259(6)	0.00552(7)
Z	0.00424(12)	0.00464(12)	0.00442(11)	0.00026(8)	0.00002(8)	0.00207(10)	0.00450(7)
B	0.0065(5)	0.0073(6)	0.0083(6)	0.0005(5)	0.0003(2)	0.0036(3)	0.0072(3)
T	0.00567(13)	0.00524(12)	0.00609(13)	-0.00050(9)	-0.00042(10)	0.00266(10)	0.00570(7)
O1	0.0071(5)	0.0071(5)	0.0073(8)	0	0	0.0035(2)	0.0072(3)
O2	0.0066(3)	0.0048(4)	0.0083(5)	0.0006(3)	0.00029(17)	0.0024(2)	0.0068(2)
O3	0.0138(5)	0.0128(4)	0.0054(4)	0.00036(19)	0.0007(4)	0.0069(3)	0.0105(2)
O4	0.0085(3)	0.0174(6)	0.0087(5)	-0.0004(4)	-0.0002(2)	0.0087(3)	0.0106(2)
O5	0.0161(6)	0.0079(3)	0.0087(5)	0.0005(2)	0.0011(4)	0.0081(3)	0.0100(2)
O6	0.0104(3)	0.0080(3)	0.0055(3)	-0.0009(2)	-0.0004(3)	0.0052(3)	0.00773(14)
O7	0.0084(3)	0.0072(3)	0.0092(3)	-0.0005(3)	-0.0024(3)	0.0015(3)	0.00938(15)
O8	0.0055(3)	0.0094(4)	0.0173(4)	0.0031(3)	0.0010(3)	0.0033(3)	0.01093(16)
H3							0.016*

*Notes:* Equivalent ( $U_{\text{eq}}$ ) and isotropic ( $U_{\text{iso}}$ ) displacement parameters; H-atom was constrained to have a  $U_{\text{iso}}$  1.5 times the  $U_{\text{eq}}$  value of the O3 oxygen.

**TABLE 4.** Selected bond distances (Å) for chromo-alumino-povondraite

<i>B</i> -O2	1.3614(12)	<i>Y</i> -O1	1.9594(9)
<i>B</i> -O8 <sup>A</sup> (× 2)	1.398(2)	<i>Y</i> -O2 <sup>B</sup> (× 2)	2.0138(7)
< <i>B</i> -O>	1.374	<i>Y</i> -O3	2.0731(12)
		<i>Y</i> -O6 <sup>C</sup> (× 2)	1.9818(8)
<i>T</i> -O4	1.6267(5)	< <i>Y</i> -O>	2.004
<i>T</i> -O5	1.6420(5)		
<i>T</i> -O7	1.5957(7)	<i>Z</i> -O3	2.0296(6)
<i>T</i> <sup>*</sup> -O6	1.6115(9)	<i>Z</i> -O6	1.9701(8)
< <i>T</i> -O>	1.619	<i>Z</i> -O8 <sup>E</sup>	1.9380(8)
		<i>Z</i> -O7 <sup>E</sup>	1.9839(8)
<i>X</i> -O2 <sup>B,F</sup> (× 3)	2.5390(14)	<i>Z</i> -O7 <sup>D</sup>	1.9504(8)
<i>X</i> -O4 <sup>B,F</sup> (× 3)	2.8126(13)	<i>Z</i> -O8	1.9519(9)
<i>X</i> -O5 <sup>B,F</sup> (× 3)	2.8127(13)	< <i>Z</i> -O>	1.971
< <i>X</i> -O>	2.694	O3-H	0.84(2)

Notes: Standard uncertainty in parentheses. Superscript letters: A = ( $y - x$ ,  $y$ ,  $z$ ); B = ( $y - x$ ,  $-x$ ,  $z$ ); C = ( $x$ ,  $x - y$ ,  $z$ ); D = ( $y - x + 1/3$ ,  $-x + 2/3$ ,  $z + 2/3$ ); E = ( $-y + 2/3$ ,  $x - y + 1/3$ ,  $z + 1/3$ ); F = ( $-y$ ,  $x - y$ ,  $z$ ). Transformations relate coordinates to those of Table 2.

\* Positioned in adjacent unit cell.

**TABLE 5.** Powder X-ray data for chromo-alumino-povondraite

$I_{(\text{meas.})}$ %	$d_{(\text{meas.})}$ Å	$d_{(\text{calc.})}$ Å	$h\ k\ l$
47	6.496	6.496	1 0 1
24	5.058	5.055	0 2 1
18	4.643	4.646	3 0 0
42	4.279	4.280	2 1 1
55	4.019	4.024	2 2 0
44	3.548	3.550	0 1 2
6	3.417	3.421	1 3 1
51	3.010	3.012	1 2 2
6	2.934	2.932	3 2 1
3	2.659	2.662	3 1 2
100	2.601	2.606	0 5 1
4	2.477	2.479	2 4 1
13	2.415	2.411	2 3 2
12	2.370	2.370	5 1 1
5	2.327	2.323	6 0 0
11	2.225	2.220	5 0 2
12	2.161	2.165	0 3 3
46	2.006	2.068	1 5 2
7	2.039	2.042	1 6 1
2	2.015	2.012	4 4 0
18	1.943	1.944	3 4 2
6	1.913	1.907	1 4 3
4	1.872	1.869	6 2 1
14	1.685	1.685	0 6 3
12	1.658	1.659	2 7 1
19	1.608	1.610	5 5 0
2	1.563	1.562	4 6 1
8	1.533	1.534	7 3 1

*Note:* Estimated errors in  $d_{(\text{meas.})}$ -spacing range from 0.01 Å for large  $d$ -values to 0.001 Å for small  $d$ -values

**TABLE 6.** Chemical composition of chromo-alumino-povondraite

	Weight %		Apfu
SiO <sub>2</sub>	34.06(08)	Si	5.96(6)
B <sub>2</sub> O <sub>3</sub> *	9.93	B	3.00
Al <sub>2</sub> O <sub>3</sub>	14.94(10)	Al	3.08(3)
Cr <sub>2</sub> O <sub>3</sub>	25.09(21)	Cr <sup>3+</sup>	3.47(4)
V <sub>2</sub> O <sub>3</sub>	1.56(37)	V <sup>3+</sup>	0.22(5)
Fe <sub>2</sub> O <sub>3</sub> <sup>†</sup>	0.10(2)	Fe <sup>3+</sup>	0.014(3)
MgO	8.65(14)	Mg	2.26(4)
CaO	0.37(9)	Ca	0.07(2)
Na <sub>2</sub> O	2.57(14)	Na	0.87(5)
K <sub>2</sub> O	0.08(4)	K	0.017(8)
F	0.45(7)	F	0.25(4)
H <sub>2</sub> O*	2.59	OH	3.02
-O=F	-0.19		
Total	100.20		

\* Calculated by stoichiometry.

† Calculated as Fe<sup>3+</sup>.

Notes: Errors for oxides are standard deviations (in brackets) of 10 spot analyses. Standard errors for the atomic proportions (in brackets) were calculated by error-propagation theory; apfu = atoms per formula unit.

**TABLE 7.** Cation site populations (apfu), mean atomic numbers and mean bond lengths (Å) for chromo-alumino-povondraite

site	site population	mean atomic number		mean bond length	
		refined	calculated	refined	calculated*
X	0.87 Na + 0.07 Ca + 0.04 □ + 0.02 K	11.49(7)	11.30		
Y	2.29 Cr <sup>3+</sup> + 0.71 Mg (2.06 Cr <sup>3+</sup> + 0.66 Mg + 0.23 V <sup>3+</sup> + 0.03 Fe <sup>3+</sup> + 0.03 Al) <sup>†</sup>	21.2(1)	21.2	2.004(1)	2.003
Z	3.04 Al + 1.54 Mg + 1.18 Cr <sup>3+</sup> + 0.22 V <sup>3+</sup> + 0.01 Fe <sup>3+</sup> (2.99 Al + 1.59 Mg + 1.42 Cr <sup>3+</sup> ) <sup>†</sup>	15.4(1)	15.3	1.971(1)	1.964
T	5.96 Si + 0.04 Al	14 <sup>‡</sup>	14.00	1.619(1)	1.620
B	3 B	5 <sup>‡</sup>	5		

Notes: apfu = atoms per formula unit;

\* Calculated using the ionic radii of Bosi and Lucchesi (2007).

<sup>†</sup> Site populations optimized by the procedure of Wright et al. (2000).

<sup>‡</sup> Fixed in the final stages of refinement

**TABLE 8.** Bond valence calculations (valence units) for chromo-alumino-povondraite.

Site	X	Y	Z	T	B	BVS
O1(W)		0.50 <sup>x3</sup> →				1.50
O2	0.14 <sup>x3</sup> ↓	0.45 <sup>x2</sup> ↓→			0.93	1.97
O3(V)		0.38	0.39 <sup>x2</sup> →			1.16
O4	0.07 <sup>x3</sup> ↓			0.99 <sup>x2</sup> →		2.05
O5	0.09 <sup>x3</sup> ↓			0.95 <sup>x2</sup> →		1.99
O6		0.49 <sup>x2</sup> ↓	0.46	1.03		1.98
O7			0.480.44	1.08		2.00
O8			0.480.50		1.02 <sup>x2</sup> ↓	2.00
BVS	0.89	2.75	2.74	4.06	2.98	
MFV	1.03	2.76	2.74	3.99	3.00	

*Note:* BVS = bond valence sum; MFV = mean formal valence from site populations



**TABLE 9.** Selected properties of oxy-dravite, chromo-alumino-povondraite and oxy-chromium-dravite

	Oxy-dravite	Chromo-alumino-povondraite	Oxy-chromium-dravite
<i>a</i> (Å)	15.9273(2)	16.0277(2)	16.0539(7)
<i>c</i>	7.2001(1)	7.3085(1)	7.3247(5)
<i>V</i> (Å <sup>3</sup> )	1581.81(4)	1625.93(5)	1634.86(15)
Space group	<i>R3m</i>	<i>R3m</i>	<i>R3m</i>
Optic sign	Uniaxial (-)	Uniaxial (-)	Uniaxial (-)
$\omega$	1.650(5)	1.745(5)	1.765(5)
$\epsilon$	1.620(5)	1.685(5)	1.715(5)
Color	Dark red	Green	Emerald Green
Pleochroism	<i>O</i> = orange <i>E</i> = pink	<i>O</i> = emerald green <i>E</i> = pale yellowish green	<i>O</i> = dark green <i>E</i> = yellow green
Ref.*	(1)	(2)	(3)

\*(1) Bosi and Skogby (2013); (2) this study; (3) Bosi et al. (2012a).

Figure 1

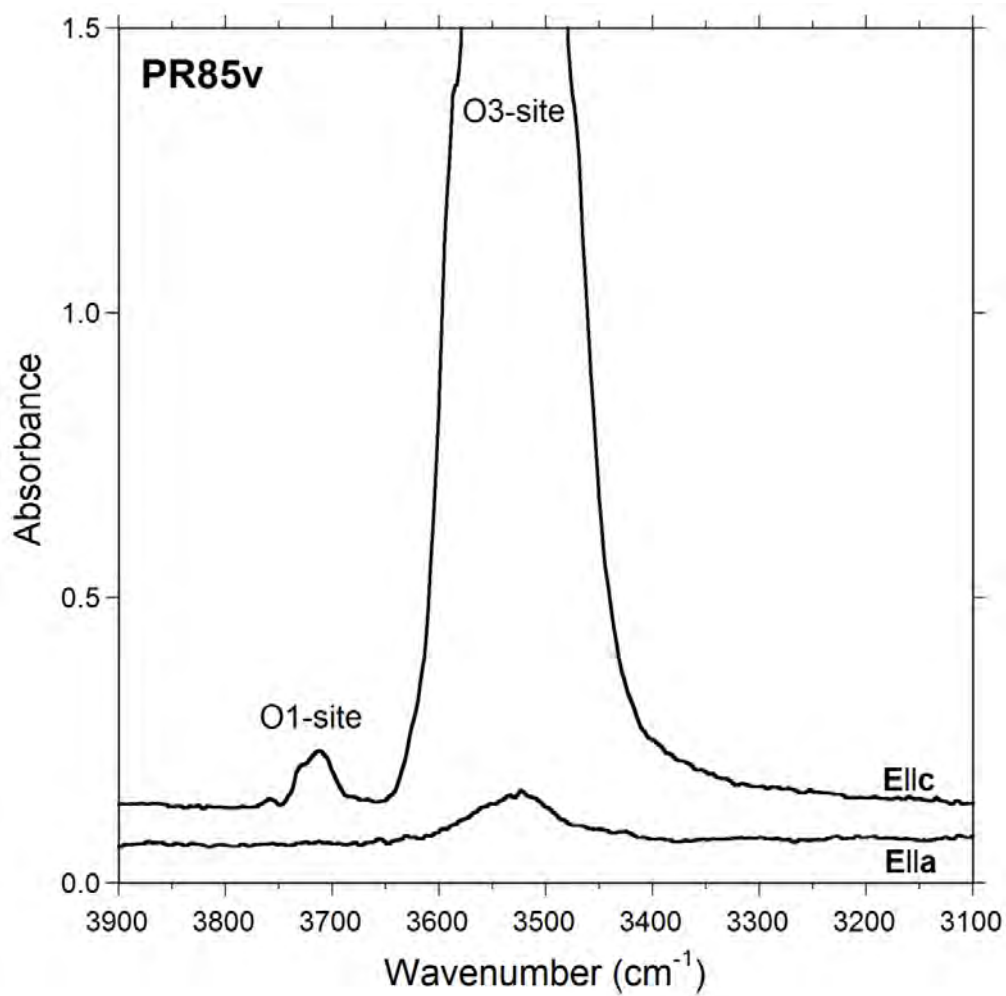


Figure 2

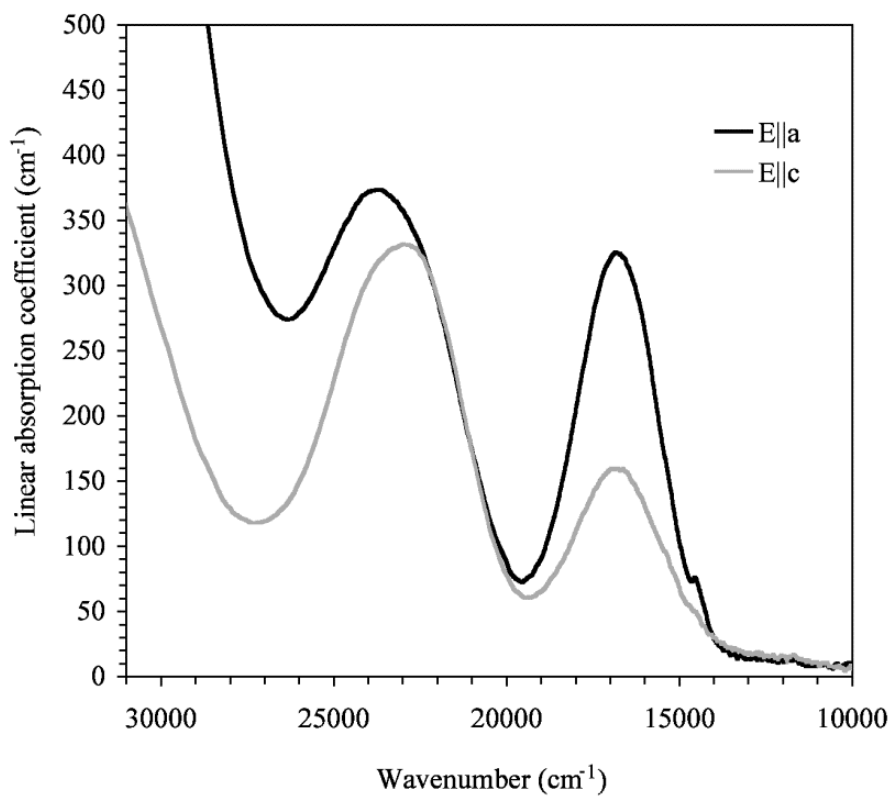


Figure 3

